

# Spectroscopic investigation of the tungsten deuteride sputtering in the EAST divertor

Q. Zhang<sup>a,b</sup>, F. Ding<sup>\*,a</sup>, S. Brezinsek<sup>c</sup>, L. Yu<sup>a,b</sup>, Y. Zhang<sup>a</sup>, P. A. Zhao<sup>a,b</sup>, D. W. Ye<sup>a,b</sup>, L. Y. Meng<sup>a</sup>, Z. H. Hu<sup>a</sup>, R. Ding<sup>a</sup>, L. Wang<sup>a</sup>, G. N. Luo<sup>a,b</sup> and EAST Team

<sup>a</sup> Institute of Plasma Physics, HFIPS, Chinese Academy of Sciences, China

<sup>b</sup> University of Science and Technology of China, China

<sup>c</sup> Forschungszentrum Jülich GmbH, Institut für Energie-und Klimaforschung-Plasmaphysik,  
Partner of the Trilateral Euregio Cluster (TEC), 52425 Jülich, Germany

\* Corresponding author: F. Ding, e-mail address: [fding@ipp.ac.cn](mailto:fding@ipp.ac.cn)

## ABSTRACT

Physical sputtering caused by particle bombardment is believed to be the main erosion mechanism of W materials in fusion devices, in which W atoms are the sputtering products. However, S. Brezinsek et al. have observed the tungsten deuteride molecule (WD) spectra in both TEXTOR and ASDEX Upgrade, and attributed it to the product of chemically assisted physical sputtering (CAPS), a new sputtering mechanism that has been proposed in recent years. In this paper, we report the spectroscopic observation on WD molecules in the EAST W divertor. The behaviors of WD molecules sputtering are compared with W atoms sputtering via the spectral measurements of the ro-vibrational band emission of WD  ${}^6\Pi \rightarrow {}^6\Sigma^+$  in the spectral range between 673 nm and 678 nm and the WI line emission at 400.9 nm. The physical sputtering characters and chemical sputtering characters of WD molecule sputtering were confirmed in EAST. The measurements in EAST showed the existence of an energy threshold for WD molecules sputtering and that the sputtering energy threshold of WD molecules is smaller than that of W atoms. Furthermore, the dependence of WD molecule sputtering efficiency (the spectral intensity normalized to the ion flux density  $j_s$  with a constant  $T_e$ ) on impact energy and heat flux were studied, presenting significantly different behaviors compared with W atom sputtering. In addition, it is found that the decrease of WD sputtering efficiency with the heat flux is accompanied with the rise of the line intensity of D $\delta$  (410.06 nm) normalized to the ion flux density  $j_s$  at the divertor target, which may imply the enhanced deuterium desorption at the W surface. The further increase of heat flux hitting the target surface could elevate the surface temperature and benefit the deuterium release from the surface, which may influence the formation of WD molecules at the surface layer.

Keywords: tungsten, plasma-facing materials, sputtering, EAST, divertor

## 1. Introduction

Tungsten (W) is selected as a plasma-facing material (PFM) for the ITER divertor due to its high melting temperature, high thermal conductivity, and low fuel retention [1-5]. However, the lifetime of the W divertor is limited by the erosion processes during plasma discharge periods. Moreover, W is a strong radiator in the core plasma, thus the central concentration of W impurity must be kept at or below  $10^{-5}$  to avoid the radiative cooling by W ions [6, 7]. Therefore, the W erosion is one of issues in fusion reactors. EAST has been equipped with W upper divertor since 2014, and W lower divertor since 2021, which helps understand the W erosion in the divertor region [8,9].

Previous research on W erosion has focused on Physical Sputtering (PS) processes caused by impinging particles [10,11]. While in 2019, S. Brezinsek and his colleagues discovered for the first time, in addition to the bare PS processes, a second W erosion mechanism in TEXTOR (limiter surfaces) and ASDEX Upgrade (divertor target plates) during deuterium plasma bombardment [4]. This mechanism has been identified as Chemically Assisted Physical Sputtering (CAPS), which leads to the formation of the tungsten deuteride molecule WD identified spectroscopically via the  ${}^6\Pi \rightarrow {}^6\Sigma^+$  transition. Measurements in TEXTOR and ASDEX Upgrade showed a dependence of the WD band emission on the surface temperature - connected to the deuterium content in the near W surface - as well as on the flux and energy of impinging energetic particles [4]. In 2020, L. Ballauf and his colleagues has observed the  $W^+$  and  $W_2^+$  of physical sputtering (PS) and  $WD^+$  of CAPS in ion beam-type experiments, and concluded that bare  $W^+$  and  $W_2^+$  were seen to be sputtered more at elevated ion impact energies and increasing surface temperatures, while the relative yield of  $WD^+$  was enhanced at higher impact energies, but diminished with increasing tungsten temperature [12]. The sputtering behavior of WD molecules is quite different from that of W atoms.

To better understand W erosion in fusion devices, here we provide further insight into the WD sputtering and W sputtering processes in EAST. The multichannel visible spectroscopy system (MVSS) allows observation and analysis of the WD band emission of the WD transition  ${}^6\Pi \rightarrow {}^6\Sigma^+$  between  $\lambda = 673$  nm and  $\lambda = 678$  nm and the neutral W line emission of the WI transition ( $5d^5({}^6S)6s^7S_3 \rightarrow 5d^5({}^6S)6p^7P_4$ ) at  $\lambda = 400.9$ nm [13]. By analyzing the intensity and position distribution of WD spectrum, some characteristics of WD sputtering under EAST experimental conditions was obtained and a comparison between WD molecules and W atoms sputtering was carried out.

Section 2 has introduced the spectroscopy system (MVSS) monitoring the W divertor region in EAST. Section 3 focuses on the similarities and differences between the sputtering behaviors of WD molecules and W atoms. In this section, the existence of energy threshold for WD sputtering is discussed and a comparison between the energy threshold of WD sputtering and that of W sputtering is carried out. Moreover, the dependences of WD and W sputtering on incident energy as well as the heat flux hitting the W target surface are also investigated. The possible reasons are suggested based on the experimental observations. In the last section, a summary is presented.

## 2. The experimental setup and relevant diagnostics

A dedicated multichannel visible spectroscopic diagnostic system has been developed for monitoring impurity behavior by collecting impurity spectra information in the divertor area in EAST [13]. There are 22 lines-of-sight (LOSs) viewing the upper outer (UO) divertor, achieving a 13 mm spatial resolution along the target surface, and 22 LOSs viewing the lower outer (LO) divertor, achieving a spatial resolution less than 25 mm, as shown in Fig. 1. The time resolution herein was normally set as about 5 ms so that 22 LOSs can be acquired simultaneously by the Electron-Multiplying Charge Coupled Device (EMCCD) detector [14]. The multichannel emission lights are transferred via optical fibers and detected simultaneously by the spectrometer with EMCCD. In addition, The ion flux density  $j_s$ , divertor electron temperature  $T_{et}$  and vertical heat flux  $q_t$  are measured by Langmuir probes (LP) on the upper and lower divertor targets [15].

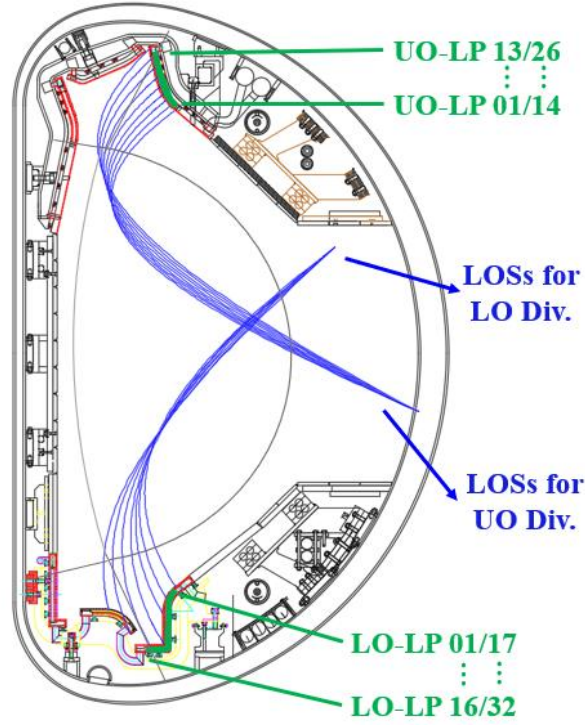


**Fig. 1.** A poloidal cross-section of EAST with the main diagnostics used in this work. The blue lines are the spectroscopic lines-of-sight (LOSs) viewing the UO and the LO divertors, and the green points are the Langmuir probes on the UO and LO divertors.

Fig. 2(a) shows the WD molecular band spectrum observed in TEXTOR [4], and Fig. 2(b) shows a typical band spectrum obtained from the UO divertor region in EAST, confirming the existence of WD molecular sputtering in EAST. The main spectroscopic features of the WD band spectrum - the line-like shape of the Q-branch at  $\lambda = 674.48\text{nm}$ , the returning R-branch at the lower wavelength end at  $\lambda = 673\text{nm}$  and the long P-branch tail in the higher range up to  $\lambda = 678\text{nm}$  - are clear. The line-like Q-branch was used as the characteristic peaks of the WD molecular band spectrum to analyze the spectral intensity and sputtering position distribution.

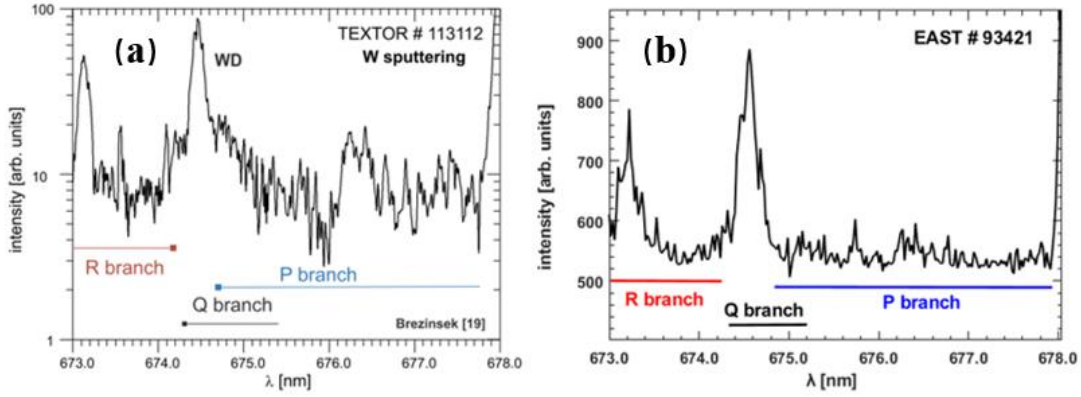


**Fig. 2.** (a) The WD molecular band spectrum observed in TEXTOR [4], and (b) the band spectrum in EAST.

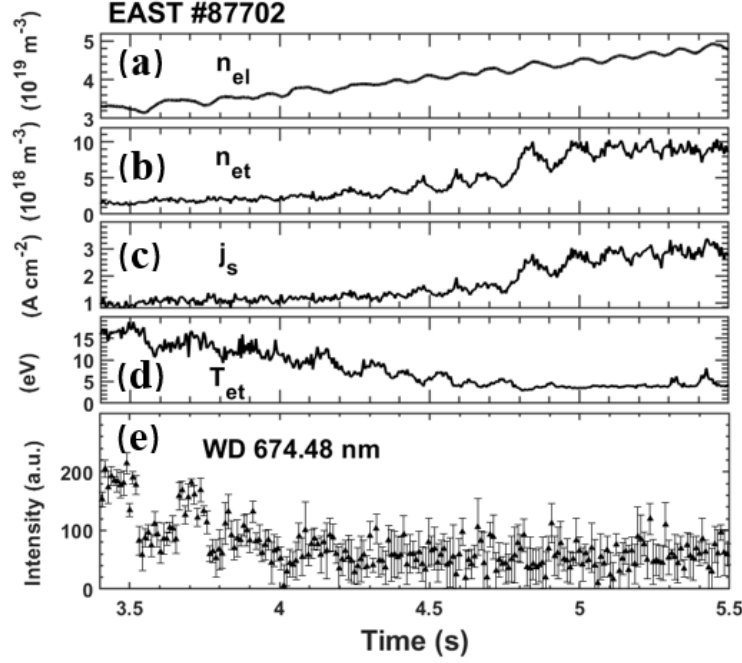
The sputtered W atom flux at divertor target can be inferred from the absolute WI photon flux by using the so-called  $S/XB$  coefficient, i.e. inverse photon efficiency method [16], which is commonly applied in the *in situ* W erosion studies [17]. However, For WD molecular sputtering, similar methods cannot be used because the so-called  $D/XB$ -values, which provides the ratio of ionization and dissociation rate coefficients (the  $D$  for decay) of the WD molecule over the excitation rate coefficient  $X$  for the observed  ${}^6\Pi \rightarrow {}^6\Sigma^+$  multiplied with the Branching ratio  $B$ , are currently unknown [4]. According to experiments and literature, The  $D/XB$  values are closely related to divertor electron temperature  $T_{et}$  [4,18,19]. We assume that within a small range of variation in  $T_{et}$ , the  $D/XB$  values for WD are comparable so that the radiant intensity normalized to the ion flux density ( $j_s$ ) -  $I_{WD}/j_s$  - can be used to discuss the quantitative changes in WD molecules sputtering. And for W atoms sputtering, the obtained  $S/XB$  values for W show that when  $T_{et} > 10\text{eV}$ ,  $I_{WI}/j_s$  can also reflect the quantitative changes in W atoms sputtering within a small range of variation in  $T_{et}$  [16]. Therefore, in this article, the changes in WD molecules sputtering and W atoms sputtering are quantitatively discussed by using the values of  $I_{WD}/j_s$  and  $I_{WI}/j_s$  under the premise that the variation range of  $T_{et}$  is small. Meanwhile, the spatial distribution of spectrum signals along the target is employed to derive the difference in sputtering characteristics between WD molecules and W atoms.

### 3. Experimental results and discussions

#### 3.1 Incident energy dependence and energy threshold for WD molecular sputtering

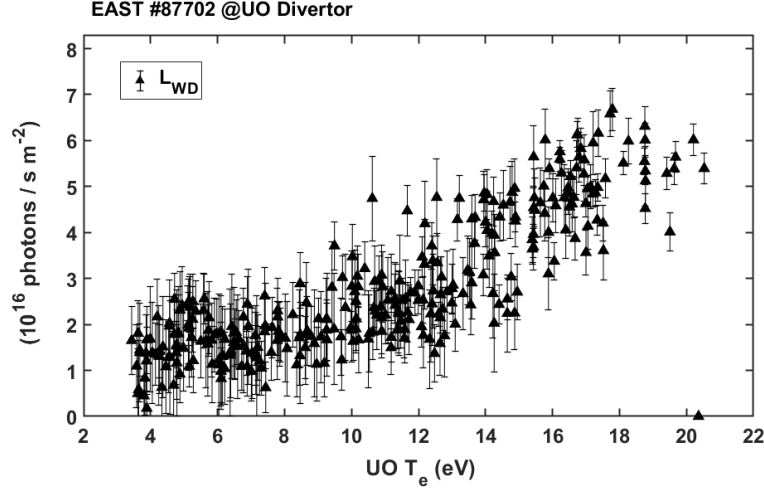
Threshold energy ( $E_{th}$ ) of impact exists for Physical Sputtering of W. For example, the  $E_{th}$  of D, He, C to sputter W from the divertor target are 220, 110 and 80 eV, respectively [20]. Experiments in non-fusion devices - ion beam-type experiments for ablation of tungsten surfaces in collisions with  $\text{Ar}^+$ ,  $\text{He}^+$  and  $\text{N}_2^+$  cation projectiles in the presence of  $\text{D}_2$  - indicate a minimum energy requirement for the chemically assisted sputtering of  $\text{WD}^+$  [12]. And for fusion devices, the release mechanism of WD

molecules is thought happen via cascades followed by a release so that the minimum impact energy is also required [4], That is to say, an energy threshold for WD sputtering should also exist. However, more details on the existence of energy threshold for WD molecular sputtering have not been studied.



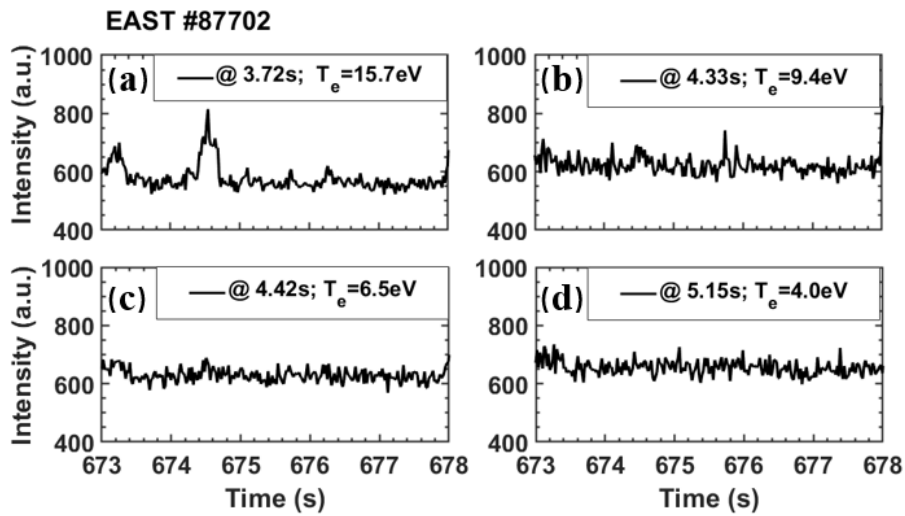
**Fig. 3.** Time evolutions of the key plasma parameter for #87702. The panels from top to bottom represent a) the plasma line-averaged density ( $\bar{n}_e$ ), b) the electron density at the UO target (UO  $n_e$ ), c) the ion flux density at the UO target (UO  $j_s$ ), d) the electron temperature at the UO target (UO  $T_e$ ) and e) the WD  ${}^6\Pi \rightarrow {}^6\Sigma^+$  band emission.

Fig. 3 shows the key plasma parameters of an L-mode discharge (#87702) in EAST, including the time evolution of the line-averaged density ( $\bar{n}_{el}$ ) in core plasma (Fig. 3(a)) as well as the electron density ( $n_{et}$ ) (Fig. 3(b)), the ion flux density ( $j_{st}$ ) (Fig. 3(c)), and the electron temperature ( $T_{et}$ ) (Fig. 3(d)) in the upper outer (UO) divertor. As  $\bar{n}_{el}$  ramps up from  $3 \times 10^{19} \text{ m}^{-3}$  to  $5 \times 10^{19} \text{ m}^{-3}$ ,  $n_{et}$  and  $j_{st}$  increases while  $T_{et}$  decreases. Fig. 3(e) shows the variation of the radiance of the line-like Q-branch of the WD  ${}^6\Pi \rightarrow {}^6\Sigma^+$  band emission and indicates that as  $j_{st}$  and  $n_{et}$  increase and  $T_e$  decreases, the WD radiance drops significantly, especially when  $T_e$  is reduced to only a few eV, the WD radiance disappears (After 4.3s, the WD radiance fluctuates at the background level, and the spectral signal measured by the spectrometer has no shape of the WD band).



**Fig. 4** WD radiance as a function of  $T_{et}$  for 87702 at UO divertor.

In order to more clearly analyze the WD radiance at low  $T_{et}$ , WD radiance as a function of  $T_{et}$  is plotted in Fig. 4. While  $T_{et}$  is a measure for the impact energy via  $E_{in} = 3k_B T_e + 2k_B T_i$  and  $T_e \approx T_i$  with the ion temperature  $T_i$  [20]. Fig. 4 shows two phenomena, one of which is that the WD radiance decreases as  $T_{et}$  decreases until around 8 eV, and the other is that WD radiance disappears when  $T_{et} < 8$  eV, although the incident particle flux is still increasing. The first phenomenon is similar to the previous observations in TEXTOR which verified the physical sputtering character of CAPS - reduction of WD with reduction of  $T_{et}$ , or more precisely impact energy  $E_{in}$ . The second phenomenon indicates that an energy threshold is existed for the WD sputtering in EAST, because the decrease of  $T_{et}$  indicates the decrease of impact energy  $E_{in}$ . When  $T_{et} < 8$  eV, the energy carried by the incident particles will not be sufficient to sputter out WD molecules.



**Fig. 5** The WD molecular band observed at the UO divertor in several seconds for 87702.

Fig. 5 shows the WD bands measured by the spectrometer at  $T_{et} = 15.7$  eV,  $T_{et} =$



9.4 eV,  $T_{et} = 6.5$  eV, and  $T_{et} = 4$  eV, respectively. When  $T_{et} < 8$  eV, the shape of the WD band does not exist, confirming that there is no WD molecular sputtering. The energy threshold requirement for WD sputtering may be related to its release mechanism – by cascading collisions [4]. Cascade collisions require enough energy to bombard the particles outside the target. It should be noted that, the energy threshold 8 eV is obtained in this shot, and may be subject to the influences of other elements, such as surface deposition layer, impurity concentration etc.

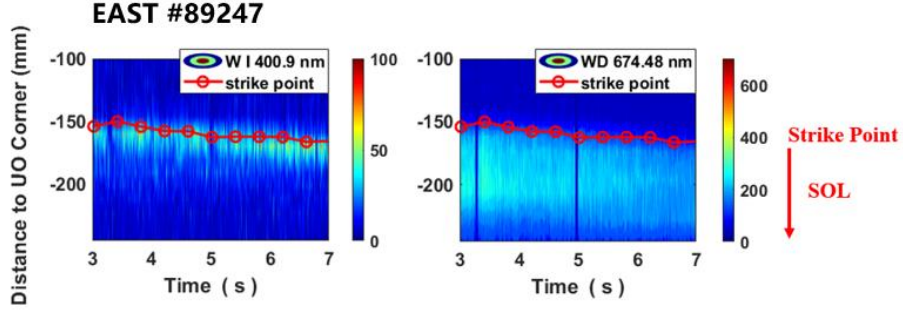


**Fig. 6** The poloidal distribution of the spectral intensity of WI and WD at the UO divertor.

Spectroscopic observations in EAST also show that the distribution range of W atom sputtering and WD molecule sputtering at the UO divertor is different. Fig. 6 shows the poloidal distribution of the spectral intensity of WI transition ( $5d^5(6S)6s^7S_3 \rightarrow 5d^5(6S)6p^7P_4$ ) and WD transition ( ${}^6\Pi \rightarrow {}^6\Sigma^+$ ) at the UO divertor during an L-mode discharge #89247, in which the red lines mark the locations of the strike point. The sputtering range of W atom is narrower and concentrated near the strike point while the sputtered WD molecules is distributed in a wider area, extending to the far Scrape-Off Layer (SOL) region. This may be due to the different sputtering energy thresholds of W atom and WD molecular, because in the SOL region farther from the strike point, the incident particle energy is lower than that near the strike point.

The discharge parameters in discharge #89247 are shown in Fig. 7 with a plasma current of  $I_p = 0.45$  MA, a plasma line-averaged density of  $\bar{n}_{el} = 1.4 \times 10^{19} \text{ m}^{-3}$  and a total input power of  $P_{in} = 1.4$  MW. As can be seen from Fig. 7(a) - (e), the parameters are stable during 3 ~ 7 s. Meanwhile, the strike point keeps at 162mm to the corner of the UO divertor during 3 ~ 7 s. Therefore, 5 different positions from strike point to farther SOL region (as shown in Fig. 7(f)) are chosen to calculate the average values of WI and WD radiance at each position during 3 ~ 7 s. The results are shown in Fig. 8.

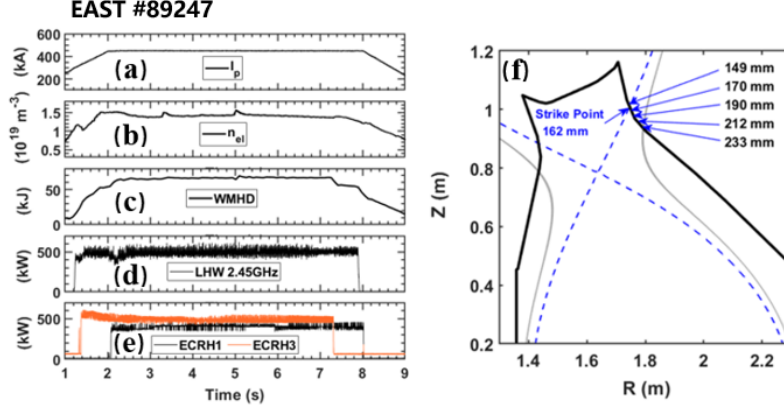


**Fig. 7** Time evolutions of (a) the plasma current, (b) the line-averaged electron density, (c) the stored energy, (d) 0.5 MW 2.45GHz LHW and (e) 0.9 MW ECRH. (f) the magnetic configuration at 4.5 s for #89247.

**Fig. 8** plots the WI and WD radiances at five different positions on the UO target. It can be seen that far from the strike point, WI radiance drops rapidly and disappears at the position of 233 mm away from the corner of UO divertor ( $T_{et} = 9.7$  eV), while the WD radiance is still strong at this position. This indicates that the sputtering energy thresholds of W atoms and WD molecules may be different, The sputtering energy threshold of WD is lower than that of W atoms. Therefore, at locations with lower impact energy, WD molecules still be sputtered, despite the disappeared W atom sputtering. Notably, the peak positions of WD and WI radiance are also different. This may be related to the distribution of heat flux incident on the divertor, which will be discussed in the next section.

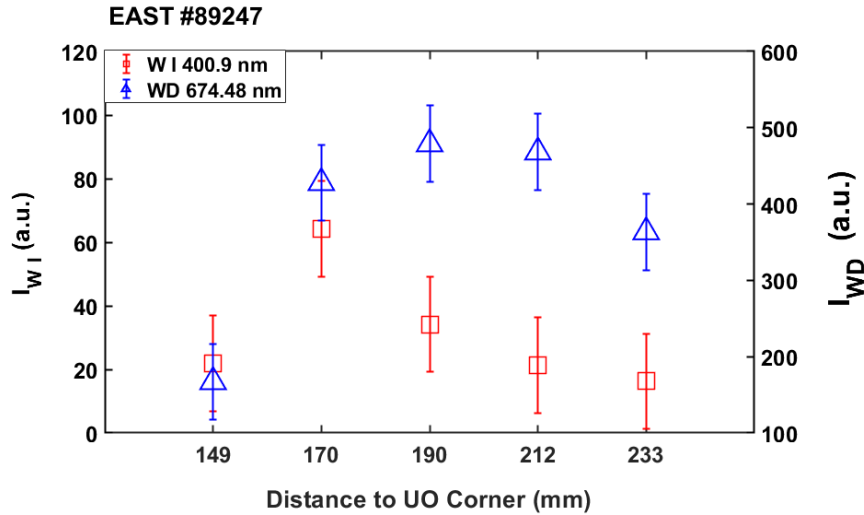


**Fig. 8** The average values of WD and WI radiance at different poloidal positions during 3~7 s of discharge #89247.

The reason for the lower energy threshold for WD sputtering is currently unclear. For carbon (C) first wall in tokamak, deuterium accumulation on the wall surface will



reduce the surface binding energy according to the research of S. G. Liu et al. [21-22]. And in the research of the irradiation of  $H^+$  on W materials, B. Yang et al. found that  $H^+$  will reduce the binding energy on the surface of the W film [23]. According to these researches,  $D^+$  bombardment and aggregation may also reduce the surface binding energy of W materials, making the bonds linking W atoms be easier to break. Gathering with a large number of  $D^+$ , the W atoms are more likely to be sputtered out of the target in the form of WD molecules. This may be the reason why there is still WD sputtering at lower impact energies, however, more detailed experiments and analysis are required to verify this conjecture.

### 3.2 Influences of heat flux and D retention

As is discussed in section 3.1, the sputtering distribution of WD molecules clearly differs from that of W atoms along the UO divertor target. Due to the varied  $T_{et}$  along the target, it is difficult to accurately compare the variation of sputtering particles of WD molecules and W atoms. According to the  $S/XB$  theory [4,14,24-26], when  $T_{et}$  remains unchanged, the change in  $I_{WI}/UO j_s$  and  $I_{WD}/UO j_s$  can reflect the change of sputtering efficiency of W atoms and WD molecules, respectively.

In a typical upper single null (USN) divertor discharge #95991,  $T_{et}$  at the peak positions of WD and WI radiance keeps almost the same from 7.2 s to 7.5 s as shown in Fig. 10(a). Thus the time range from 7.2 s – 7.5 s in #95991 is used to compare the variation of the sputtering efficiency of WD molecules and W atoms.

Discharge #95991 is sustained by 2 MW LHW, 0.9 MW ECRH and 2 MW NBI heating power at a line-averaged density of  $\bar{n}_{el} = 3 \times 10^{19} \text{ m}^{-3}$ . The distribution of the ion flux density ( $UO j_s$ ), as well as WI and WD radiance along the W target in this discharge are shown in Fig. 9. It can be seen that the WI radiance is mostly concentrated near the strike point, consistent with the distribution of the  $UO j_s$ . While the peak WD radiance is farther away from the strike point, where the  $UO j_s$  is obviously weaker.

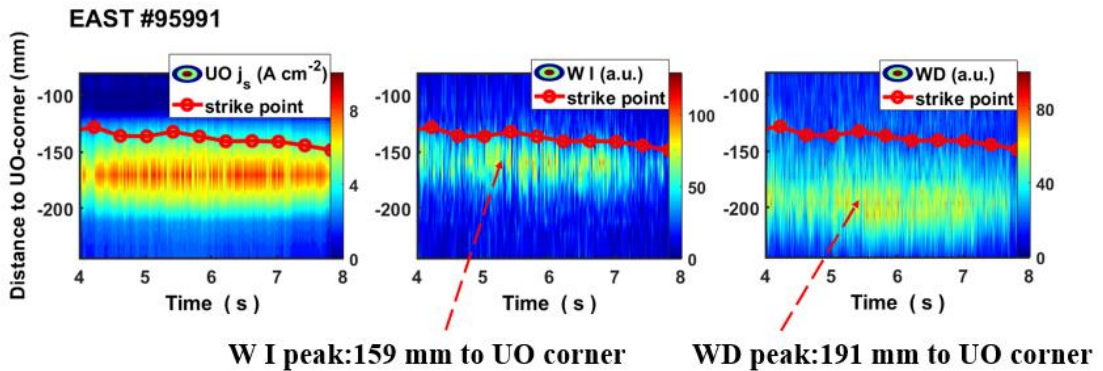
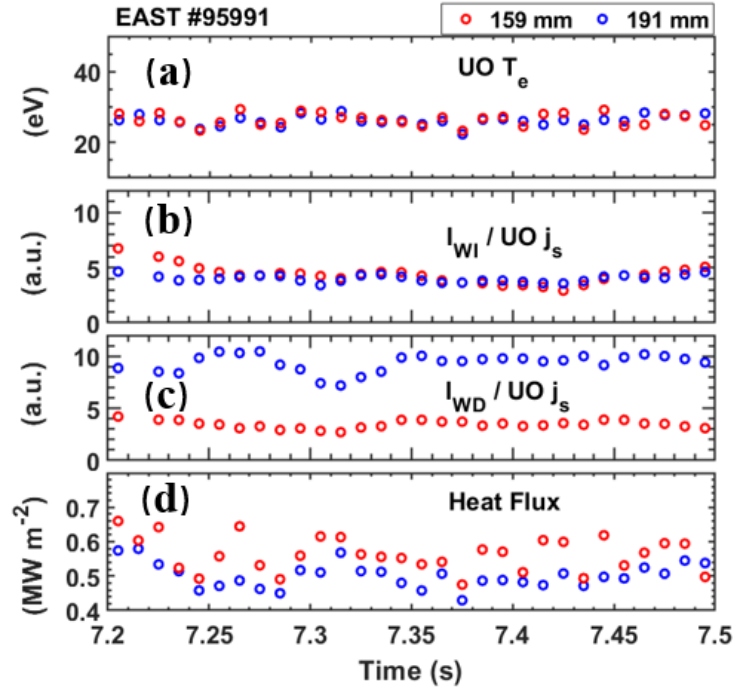


Fig. 9 The distribution of the ion fluxes ( $UO j_s$ ), as well as WI and WD radiance along the W target of discharge #95991.

Fig. 10 compare the temporal evolution of main parameters from 7.2 s ~ 7.5 s at 159 mm and 191 mm. Fig. 10(a) shows that during 7.2 s ~ 7.5 s, the  $T_{et}$  at these two

positions are equal, which means the same impact energy  $E_{in}$ . The same  $I_{WI}/UO j_s$  at 159 mm and 191 mm in Fig. 10(b) indicates the same sputtering efficiency of W atoms at the two positions, demonstrating a pure physical sputtering characteristic, i.e. the dependence on  $T_e$ . By contrast, Fig. 10(c) shows that higher sputtering efficiency of WD molecules appears at 191 mm despite the same  $T_{et}$  at the two positions. There should be some element other than impact energy influencing the WD sputtering efficiency. Fig. 10(d) compares the heat flux at the two positions [27,28]. The heat flux at 191 mm is around 0.5 MW/m<sup>2</sup>, lower than 0.6 MW/m<sup>2</sup> at 159 mm. Normally, higher heat flux would lead to higher target temperature which could influence the D content in the thin surface layer [29].



**Fig. 10** Time evolutions of (a) the electron temperature ( $T_{et}$ ), (b) the ratio  $I_{WI}/j_s$ , (c) the ratio  $I_{WD}/j_s$  of the two positions (159 mm and 191 mm away from the UO divertor corner). And time evolutions of (d) the heat flux of the two positions.

The influences of heat flux on the sputtering efficiency of WD molecules and W atoms were also compared on the temporal evolution. The H-mode discharge #98765 is with lower single null (LSN) configuration and sustained by 2.5 MW LHW and 1.45 MW ECRH. The plasma current  $I_p$  at the top phase is 500 kA and lasts 20 s. The line-averaged electron density  $\bar{n}_{el}$  slowly rises from  $1.6 \times 10^{19} \text{ m}^{-3}$  to  $2.5 \times 10^{19} \text{ m}^{-3}$  as shown in Fig. 11(a). Fig. 11(b) and (c) show an increasing particle flux density (LO  $j_s$ ) and decreasing electron temperature (LO  $T_e$ ) at the lower outer divertor with the increasing of electron density  $\bar{n}_{el}$ . During 9 ~ 15 s, the heat flux hitting the divertor drops from 1.3 MW m<sup>-2</sup> to 0.3 MW m<sup>-2</sup> (Fig. 11(d)).

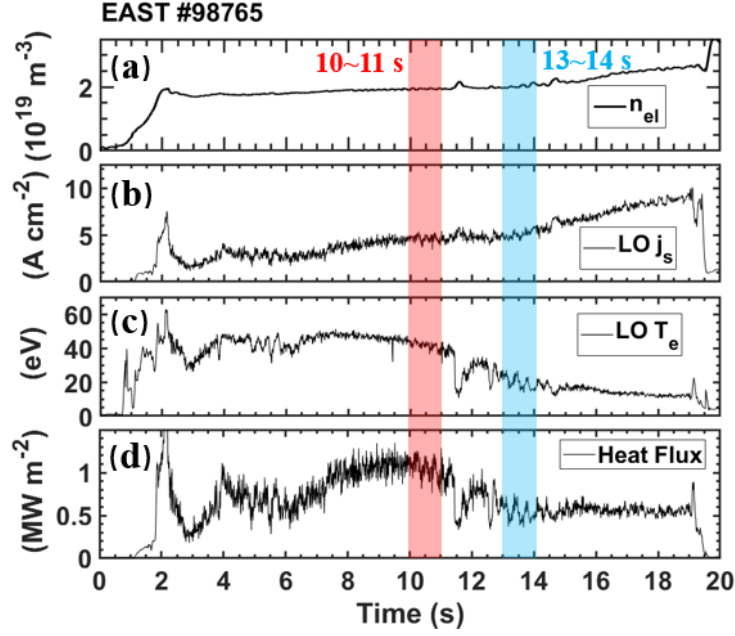


**Fig. 11** Time evolutions of (a) the line-averaged electron density  $\bar{n}_{el}$  in the core plasma, (b) the particle flux density ( $j_s$ ), (c) the electron temperature ( $T_e$ ) and (d) the heat flux in the lower outer (LO) divertor of discharge #98765.

To minimize the influence of  $T_e$  on the photon emission efficiency, two periods in the discharge with relative constant  $T_e$  are selected for analysis as shown in Fig. 12. Both WD molecule and W atom sputtering present similar rising trend with the heat flux when the heat flux is low ( $0.3 \text{ MW/m}^2 \sim 0.6 \text{ MW/m}^2$  in Fig. 12(a)). When the heat flux rises to above  $0.6 \text{ MW/m}^2$ , a downward trend of WD sputtering efficiency can be observed with increasing heat flux while W atom sputtering efficiency still keeps a rising trend with the heat flux, suggesting different sputtering mechanism for WD molecule sputtering compared with W atom sputtering.

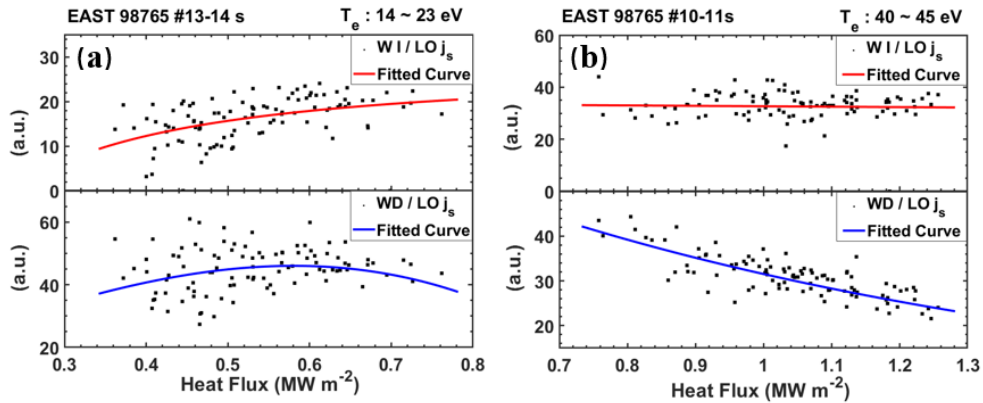
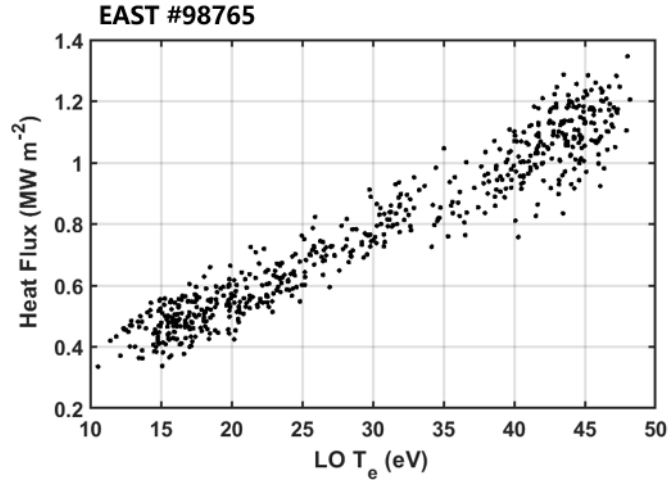


**Fig. 12** The evolution of  $I_{WI}/LO j_s$  and  $I_{WD}/LO j_s$  as a function of heat flux hitting the LO divertor (a) during 13 s to 14 s and (b) during 10 s to 11 s.

Fig. 12(a) shows the evolution of  $I_{WI}/LO j_s$  and  $I_{WD}/LO j_s$  as functions of heat flux

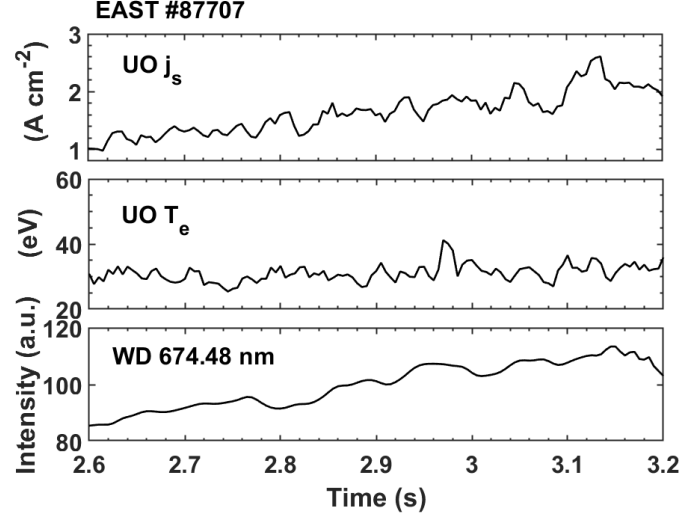
during 13 ~ 14 s when the value of heat flux is relatively low and LO  $T_e$  changes in the range of 14 ~ 23 eV. Assume that the  $S/XB$ -values for WI and the  $D/XB$ -values for WD are respectively comparable in the range of LO  $T_e = 14$  eV and LO  $T_e = 23$  eV [4,16]. So that the ratio  $I_{WI}/LO j_s$  and  $I_{WD}/LO j_s$  can represent the sputtering efficiency of W atoms and WD molecules in this period. As the heat flux increases, the sputtering efficiency of W atoms keeps increasing while the sputtering efficiency of WD molecules increases first and then decreases after reaching a peak.

Fig. 12(b) shows the evolution of  $I_{WI}/LO j_s$  and  $I_{WD}/LO j_s$  as functions of heat flux during 10 ~ 11 s when the value of heat flux is relatively high and LO  $T_e$  changes in the range of 40 ~ 45 eV. In this phase, as the heat flux increases, the sputtering efficiency of W atoms remains at a high level, while the sputtering efficiency of WD molecules significantly reduces. The results may be the influence of the chemical sputtering character of WD sputtering - the WD sputtering has a significant dependence on the deuterium content in the W surface layer [4]. The increasing surface temperature of the W target caused by the increasing heat flux can lead to more desorption of the deuterium in the surface layer [30,31], which may be the possible reason for the decrease of the sputtering efficiency of WD molecules. While for W atoms, since it is purely physical sputtering, its sputtering efficiency is mainly affected by the impact energy. Therefore, in Fig. 12(a) its sputtering efficiency continues to rise due to the rise of LO  $T_e$ , and in Fig. 12(b) its sputtering efficiency remains at a high level since LO  $T_e$  remains at a high level (The relationship between LO  $T_e$  and heat flux of discharge #98765 in LO divertor is shown in Fig. 13).



**Fig. 13** The relationship between LO  $T_e$  and heat flux of discharge #98765 in LO divertor.

It is observed in EAST that the decrease of the sputtering efficiency of WD with the increase of the heat flux hitting the W target is often accompanied with the rise of the line intensity of  $D_\delta$  (410 nm) normalized to the ion flux density ( $j_s$ ) at the divertor, which may imply the enhanced D desorption at the W surface.



**Fig. 14** Time evolution of the ion flux ( $j_s$ ), the electron temperature ( $T_e$ ), and the WD radiance in the upper outer (UO) divertor of discharge #87707

**Fig. 14** shows the evolution of the ion flux density ( $j_s$ ), the electron temperature ( $T_e$ ), and the WD radiance in the upper outer (UO) divertor of discharge #87707 during 2.6 s to 3.2 s. In this phase the ion flux density  $UO j_s$  keeps increasing with time while the electron temperature  $UO T_e$  remains almost unchanged, therefore the heat flux increases with time.

During the phase with constant  $UO T_e$ , the ratio  $I_{WD}/UO j_s$  and  $I_{D\delta}/UO j_s$  can qualitatively reflect the sputtering efficiency of WD molecules and the deuterium desorption rate at the divertor target. A higher ratio  $I_{D\delta}/UO j_s$  may mean the increased deuterium evaporation/dissociation from the W surface layers, thus a lower deuterium retention ratio in the W target [30,31].

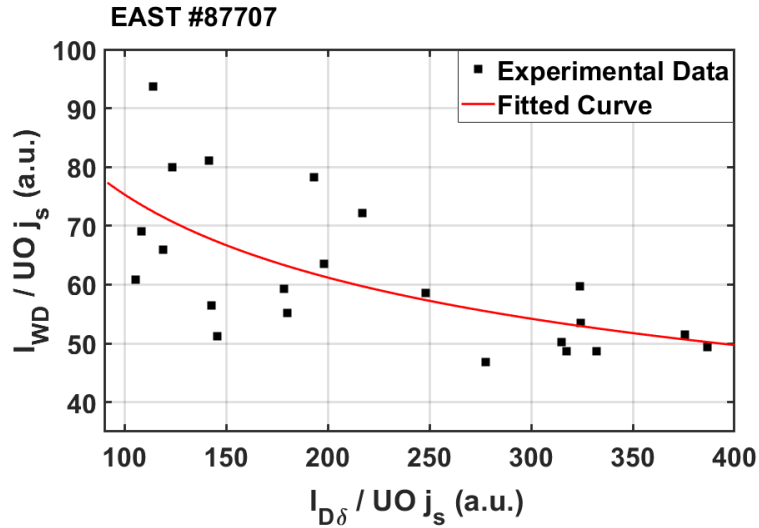


**Fig. 15** The relationship between the ratio  $I_{WD}/UO j_s$  and  $I_{D\delta}/UO j_s$  during 2.6s to 3.2s.

**Fig. 15** plots the ratio  $I_{WD}/UO j_s$  against  $I_{D\delta}/UO j_s$  from 2.6 s to 3.2 s in #87707 when the  $T_{et}$  keeps nearly constant. It can be seen that  $I_{WD}/UO j_s$  presents a decreasing trend with  $I_{D\delta}/UO j_s$ , indicating that the sputtering efficiency of WD molecules

decreases with the reduction of deuterium retention in the W target. The increasing  $I_{D\delta}/UO j_s$  should be resulted from the increasing heat flux. The increase of heat flux could elevate the surface temperature and benefit the deuterium release from the W surface, which may influence the formation of WD molecules at the W surface layer. Therefore, the changes in deuterium content in the W surface layers may be responsible for the dependence of WD sputtering on the heat flux hitting the W divertor, which is consistent with research result of S.Brezinsek.et.al [4]. the near-surface fuel content in W may affect the WD sputtering efficiency - the chemical sputtering character of CAPS. Different D content in the W surface at different target temperature could play an important role here.

#### 4. Summary and conclusion

WD molecule sputtering is observed via spectroscopic measurement in the EAST W divertor and compared with W atom sputtering by defining  $I_{WD}/j_s$  and  $I_{WI}/j_s$  as the sputtering efficiencies of WD molecules and W atoms, respectively. The dependences of  $I_{WD}/j_s$  on target  $T_{et}$  is obtained and an energy threshold of 8 eV is found for WD molecule sputtering in the observed discharge. Experimental comparison shows that the sputtering of W atoms is mostly concentrated near the strike point, while the sputtering distribution of WD molecules is relatively wide, extending to the far SOL region where impact energy of incident ions is lower than that around the strike point. These indicate that the sputtering energy threshold of WD molecules in EAST is smaller than that of W atoms.

The other important difference between WD molecule sputtering and W atom sputtering is the dependence on heat flux hitting the W target. When the heat flux increases, the sputtering efficiency of WD molecules first increases and then decreases, while the sputtering efficiency of W atoms continues to increase with the heat flux. The similar dependences of the sputtering efficiency of WD molecules and W atoms are also found on target  $T_{et}$ , due to the proportional relationship between heat flux and  $T_{et}$ . These observations indicate that in addition to the impact energy ( $T_{et}$ ), there is other element influencing WD sputtering efficiency, which is different from W atom sputtering efficiency, a typical physical sputtering with a mere dependence on the impact energy ( $T_{et}$ ). Further study shows that the WD sputtering efficiency has a decreasing trend with the increasing of deuterium desorption rate. This could imply that the near-surface fuel content in W may be another important factor influencing the WD sputtering efficiency. The decreasing WD molecule sputtering efficiency with increasing heat flux is most likely due to the reduced deuterium content in the W surface layer caused by the increased heat flux, thus the elevated target temperature. So the WD molecule sputtering could be ascribed to the chemically assisted physical sputtering.

#### Acknowledgments

This work was supported by the National Key Research and Development Program



of China (Grant Nos. 2017YFE0301300, 2017YFA0402500, and 2018YFE0303103), the National Natural Science Foundation of China (Grant Nos. 12192283 and 12022511), the JSPS-CAS Bilateral Joint Research Project (Grant No. GJHZ201984), and the Key Research Program of Frontier Sciences of CAS (Grant No. ZDBS-LY-SLH010).

## References

- [1] S. P. T. Hirai, et al., *Nuclear Materials and Energy* 9 (2016) 616-622.
- [2] R. Neu, et al., *Physica Scripta* T138 (2009) 014038.
- [3] R. Neu, et al., *Physics of Plasmas* 20 (2013) 056111.
- [4] S. Brezinsek, et al., *Nuclear Materials and Energy* 18 (2019) 50-55.
- [5] A. Kirschner, et al., *Nuclear Materials and Energy* 18 (2019) 239-244.
- [6] T. Pütterich, et al., *Nuclear Fusion* 50 (2010) 025012.
- [7] I. Murakami, et al., *Nuclear Materials and Energy* 26 (2021) 100923.
- [8] Lei Cao, et al., *J Fusion Energ.* 34 (2015) 1451–1456.
- [9] G.S. Xu, et al., *Nucl. Fusion* 61 (2021) 126070.
- [10] X. H. Chen, et al., *Nucl. Fusion* 61 (2021) 046046.
- [11] M. Mayer, et al., *Journal of Nuclear Materials* 363–365 (2007) 101–106.
- [12] L. Ballauf, et al., *International Journal of Mass Spectrometry* 448 (2020) 116252.
- [13] H. Mao, et al., *Rev Sci Instrum*, 88 (2017) 043502.
- [14] H. Mao, et al., *Nuclear Materials and Energy*, 12 (2017) 447-452.
- [15] J.C. Xu, et al., *Rev Sci Instrum*, 87 (2016) 083504.
- [16] R. Neu, et al., *AIP Conference Proceedings* 901, 85 (2007).
- [17] T. Abrams, et al., *Physics of Plasmas* 26 (2019) 062504.
- [18] H. Kawazome, et al., *Plasma and Fusion Research* 5 (2010) S2073.
- [19] T. Nakano, et al., *Nuclear Fusion* 42 (2002) 689-696.
- [20] P.C. Stangeby, *The Plasma Boundary of Magnetic Fusion Devices*. (2000).
- [21] S. Liu, et al., *Journal of Applied Physics* 108 (2010) 073302.
- [22] E. Salonen, et al., *Physical Review B* 63 (2001) 195415.
- [23] B. Yang, et al., *Chinese Journal of Atomic and Molecular Physics* 19 (2002) 42-44.
- [24] A. Pospieszczyk, et al., *J. Phys. B: At. Mol. Opt. Phys.* 43 (2010) 144017.
- [25] G.-N. Luo, et al., *Nucl. Fusion* 57 (2017) 065001.
- [26] D. Nishijima, et al., *Plasma Physics and Controlled Fusion* 50 (2008) 125007.
- [27] L.Y. Meng, et al., *Plasma Physics and Controlled Fusion* 62 (2020) 065008.
- [28] L. Wang, et al., *Nuclear Fusion* 59 (2019) 086036.
- [29] C. Sang, et al., *Nuclear Fusion* 52 (2012) 043003.
- [30] C. Sang, et al., *EPS2011 38th Conference on Plasma Physics*. (2011) P5.058.
- [31] J. Roth, et al., *Physica Scripta* 145 (2011) 014031.